Four basic residues critical for the ion selectivity and pore blocker sensitivity of TMEM16A calcium-activated chloride channels

Christian J. Peters[a], Haibo Yu[b,c], Jason Tien[a], Yuh Nung Jan[a,d], Min Li[b,1], and Lily Yeh Jan[a,d,2]

[a]Department of Physiology and [d]Howard Hughes Medical Institute, University of California, San Francisco, CA 94158; [b]The Solomon H. Snyder Department of Neuroscience, High-Throughput Biology Center and Johns Hopkins Ion Channel Center, Johns Hopkins University, Baltimore, MD 21205; and [c]State Key Laboratory of Bioactive Substances and Functions of Natural Medicines, Institute of Materia Medica, Chinese Academy of Medical Sciences and Peking Union Medical College, Beijing 100050, China

Contributed by Lily Yeh Jan, February 5, 2015 (sent for review January 3, 2015; reviewed by Eitan Reuveny)

TMEM16A (transmembrane protein 16) (Anoctamin-1) forms a calcium-activated chloride channel (CaCC) that regulates a broad array of physiological properties in response to changes in intracellular calcium concentration. Although known to conduct anions according to the Eisenman type I selectivity sequence, the structural determinants of TMEM16A anion selectivity are not well-understood. Reasoning that the positive charges on basic residues are likely contributors to anion selectivity, we performed whole-cell recordings of mutants with alanine substitution for basic residues within the putative pore region and identified four residues on four different putative transmembrane segments that significantly increased the permeability of the larger halides and thiocyanate relative to that of chloride. Because TMEM16A permeation properties are known to shift with changes in intracellular calcium concentration, we further examined the calcium dependence of anion selectivity. We found that WT TMEM16A but not mutants with alanine substitution at those four basic residues exhibited a clear decline in the preference for larger anions as intracellular calcium was increased. Having implicated these residues as contributing to the TMEM16A pore, we scrutinized candidate small molecules from a high-throughput CaCC inhibitor screen to identify two compounds that act as pore blockers. Mutations of those four putative pore-lining basic residues significantly altered the IC_{50} of these compounds at positive voltages. These findings contribute to our understanding regarding anion permeation of TMEM16A CaCC and provide valuable pharmacological tools to probe the channel pore.

calcium-activated channels | chloride channels | channel pharmacology | TMEM16A | ion channel biophysics

The TMEM16 (transmembrane protein 16) family consists of transmembrane proteins, of which at least two members, TMEM16A and TMEM16B, are pore-forming subunits of calcium-activated chloride channels (CaCCs) (1–4). TMEM16A and TMEM16B channels serve a variety of functions in many cell types, including secretory epithelia (5–8), gastrointestinal pacemakers (9), sensory neurons and hippocampal neurons (10–13), urethral and vascular smooth muscle (14, 15), and tumor cells (16). Hence, it is important to understand how these channels work.

TMEM16A channels are activated by direct binding of intracellular calcium ions (17–19) and open to conduct currents with anion selectivity that follows an Eisenman type I sequence (1, 3); however, the mechanism of permeation in TMEM16A channels is not well-understood. Although binding of intracellular calcium at physiological concentrations is known to catalyze the passage of anions through the channel, the properties of the resulting conductance are complex. A hallmark feature of CaCC in multiple cell types, including *Xenopus* oocytes, is the presence of two obvious conduction modes: a voltage-dependent or outwardly rectifying mode at lower concentrations of calcium and a leak mode with Ohmic character at higher concentrations (20, 21). Whereas this phenomenon may reflect voltage-dependent calcium sensitivity of CaCC, it may also indicate the existence of multiple open states (20, 22–24). Indeed, *Xenopus* TMEM16A (3) and mouse TMEM16B (25) appeared to adopt multiple distinguishable conductive conformations as intracellular calcium levels increased after photolysis of caged calcium. Furthermore, the identity of the permeating anions also seems to influence gating behavior, because anions for which the channel shows preferred selectivity also seem to facilitate CaCC activation in both *Xenopus* oocytes (23) and cells heterologously expressing mouse TMEM16B (26). Taken together, these findings suggest that the anion pore and the calcium-dependent gating machinery may be tightly coupled to one another, whereby increases in intracellular calcium may modify chloride-binding properties in the pore. These observations further raise the question of whether the molecular determinants of anion selectivity may vary in different distinct open states that may be occupied preferentially at various intracellular calcium levels. In light of these considerations, it is intriguing that a recently published crystal structure of a TMEM16 family protein from the *Nectria hematococcus* fungus, although not showing obvious channel behavior itself, has a calcium-binding pocket in close physical proximity to the fifth transmembrane helix, which harbors a residue corresponding to K584 of TMEM16A and Q559 of TMEM16F (27). This residue has been implicated to underlie the differences in ion selectivity between the TMEM16A and TMEM16F channels, because the anion selectivity of TMEM16A is reduced by the

Significance

TMEM16A is a calcium-activated chloride channel, meaning that it is a protein found at the surface of a variety of cells that permits chloride to enter when internal calcium levels rise. TMEM16A has been implicated in a variety of biological processes, including epithelial fluid secretion, smooth muscle contraction, neuron firing, and cancer cell proliferation. However, it is unclear how chloride ions are guided across the cell membrane by this protein. Here, we have modified and tested positively charged amino acids of TMEM16A and found four that modify chloride flux. We also tested potential blockers from a high-throughput screen and describe two that appear to block chloride's path, which should contribute to future studies attempting to further analyze TMEM16A's function.

Author contributions: C.J.P., H.Y., Y.N.J., M.L., and L.Y.J. designed research; C.J.P., H.Y., and J.T. performed research; C.J.P., H.Y., J.T., and M.L. contributed new reagents/analytic tools; C.J.P. and H.Y. analyzed data; and C.J.P., H.Y., J.T., and L.Y.J. wrote the paper.

Reviewers included: E.R., Weizmann Institute of Science.

The authors declare no conflict of interest.

[1]Present address: GlaxoSmithKline, King of Prussia, PA 19406.

[2]To whom correspondence should be addressed. Email: Lily.Jan@ucsf.edu.

This article contains supporting information online at www.pnas.org/lookup/suppl/doi:10.1073/pnas.1502291112/-/DCSupplemental.

K584Q mutation and the cation selectivity of TMEM16F is reduced by the Q559K mutation (28).

It is important to delineate the location and properties of the pore of TMEM16A channels. Whereas the TMEM16A pore has been proposed to be between the fifth and sixth of either 8 (17, 19, 29) or 10 transmembrane segments (27) and several positively charged residues were proposed to contribute to pore properties (1, 2), whether and how these residues influence permeation remain unclear as the channel's topological arrangement has come into clearer focus using biochemical, biophysical, and structural biological methods (17, 19, 27, 29). It is also important to identify and characterize pharmacological modulators of the TMEM16A channel pore. Of the channel blockers that have been identified, some are of low potency [DIDS and tannic acid (30)] and/or nonspecific [niflumic acid, anthracene-9-carboxylic acid, NPPB, CaCC-inh001, and benzbromarone (6, 31–33)], whereas others with potency in the low micromolar range (30, 34) seem to be only partially effective (T16Ainh-001) in blocking the current (31), and none have been conclusively shown to interact with the pore.

To address these questions, we used two approaches to examine TMEM16A permeation behavior. First, reasoning that positively charged residues are likely involved in conferring anion selectivity to TMEM16A, we mutated all of the basic residues within the putative pore region as well as several others previously queried by Martinez–Torres and coworkers (35) for contribution to apparent anomalous mole fraction effects and in helices shown to reside nearby in the fungal TMEM16 crystal structure (27), and we screened for those that prevented shifts in anion selectivity with higher intracellular calcium. Second, we tested compounds isolated from a high-throughput small molecule screen based on iodide quenching of YFP fluorescence (2, 34, 36) to search for pore blockers. From these compounds, we identified two with voltage- and anion-dependent blocking properties that appeared to display some preference for specific open states, because they blocked the channel with greater potency at elevated intracellular calcium. Here, we report that alanine substitution for four basic residues caused not only alterations of anion selectivity but also, shifted the concentration dependence of these pore blockers, suggesting that the affinity between the pore and the blockers was being affected by those mutations of putative pore-lining residues.

Results

By comparing the amino acid sequence of mouse TMEM16A (National Center for Biotechnology Information accession no. NP_848757.4) with the recent predictions of channel topology (17, 19, 29) and the crystal structure of a fungal ortholog (27), we identified seven basic amino acids in the putative pore region that were also conserved in the highly similar TMEM16B channel (National Center for Biotechnology Information accession no. NP_705817.2). Based on 3D proximity in the crystal structure (27) and previous studies on channel permeation (35), we considered an additional five basic residues from transmembrane segments

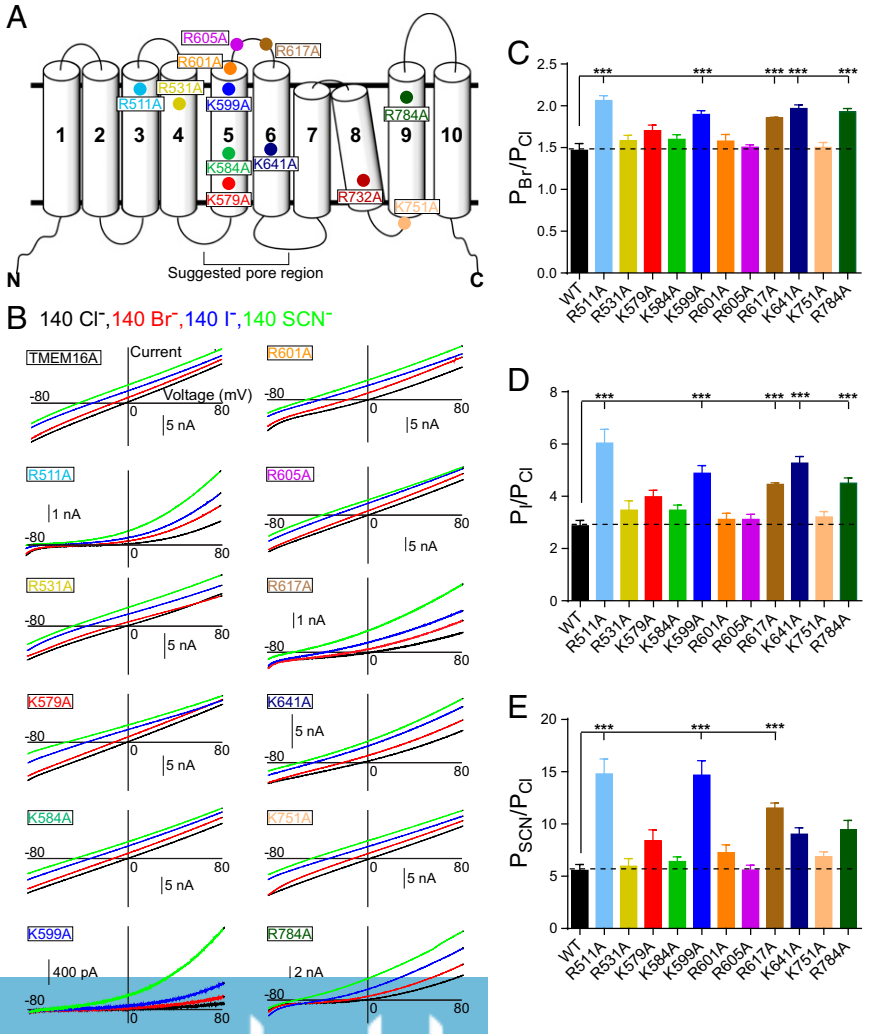

Fig. 1. Alanine scan of putative pore-lining basic residues identifies five that significantly increase permeability ratios in bi-ionic condition. (*A*) Proposed topology of TMEM16A channel with basic residues within the putative pore region or previously implicated in permeation indicated at their predicted locations. (*B*) Representative currents recorded from voltage ramps from –80 to +80 mV in whole-cell patch clamp in the constructs indicated. Color coding indicates extracellular ion species (all at 140 mM). Black, NaCl; blue, NaI; green, NaSCN; red, NaBr. Permeability ratios for all alanine mutants as determined by solving the Goldman–Hodgkin–Katz voltage equation for (*C*) bromide, (*D*) iodide, and (*E*) thiocyanate compared with chloride for each construct. Ratios are compared using one-way ANOVA followed by Tukey's posthoc test. Statistical comparison of WT TMEM16A in whole-cell mode with other constructs is indicated with the top bar. ***Significant difference ($P < 0.001$).

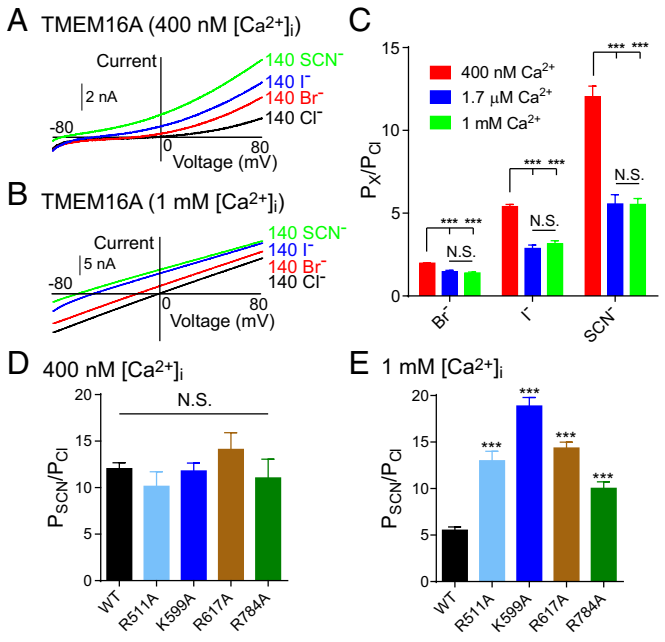

Fig. 2. Ca^{2+} dependence of anion selectivity for TMEM16A is abolished by mutations of basic residues. (*A*) Currents recorded from voltage ramps from −80 to +80 mV in WT TMEM16A in whole-cell patch clamp with 400 nM Ca^{2+} in the pipette. Intracellular solution contained 140 mM NaCl, whereas extracellular ion concentrations are as indicated. (*B*) Currents recorded from voltage ramps from −80 to +80 mV in WT TMEM16A with 1 mMCa^{2+} in the pipette. (*C*) Permeability ratios are determined by solving the Goldman–Hodgkin–Katz voltage equation for each solution compared with chloride in the indicated concentrations of Ca^{2+}. Permeability ratios for thiocyanate over chloride are shown for alanine mutants at (*D*) 400 nM Ca^{2+} and (*E*) 1 mM Ca^{2+}. N.S., not significant. ***$P < 0.001$.

3–9. These 12 residues are indicated on the channel schematic in Fig. 1*A* [residue numbering as in splice variant 'a' (37) and helix numbering as in ref. 27] and were each mutated to alanine to assess their contributions to anion selectivity. When ramp protocols (from −80 to +80 mV) were applied to WT TMEM16A channels transiently expressed in HEK293 cells at an intracellular calcium concentration $[Ca^{2+}]_i$ of 1.7 μM, whole-cell recording yielded a nearly linear, nonrectifying current (Fig. 1*B*). When extracellular chloride is replaced with chloride to bromide (Fig. 1*B*, red), iodide (Fig. 1*B*, blue), or thiocyanate (Fig. 1*B*, green), a leftward shift in the reversal potential (E_{Rev}) takes place, reflecting the higher selectivity of the channel for those ions compared with chloride (Fig. 1*B*). By solving the Goldman–Hodgkin–Katz voltage equation (see *SI Extended Data Analysis*), we determined the permeability ratios over chloride for bromide ($P_{Br}/P_{Cl} = 1.5 \pm 0.1$), iodide ($P_I/P_{Cl} = 2.9 \pm 0.2$), and thiocyanate ($P_{SCN}/P_{Cl} = 5.6 \pm 0.6$) under these conditions. Using the same recording conditions, we then tested mutants with alanine substitutions at the 12 residues shown in Fig. 1*A*, of which 11 showed large enough currents for accurate measurements of voltage shifts. We then plotted the permeability ratios from each mutant for each ion and compared them with the WT (Fig. 1 *C*–*E*). From these 11 residues, we identified 5 that produced significant shifts in E_{Rev} with Br^- and I^- ($P < 0.05$ using one-way ANOVA). Surprisingly, these residues are not localized to one membrane domain but appeared to be found on several different putative transmembrane segments; they included R511 from TM3, K599 from TM5, R617 from the TM5-6 linker, K641 from TM6, and R784 from TM9. Three of these mutants also produced shifts with SCN^- that also reached statistical significance. As mentioned earlier, one mutant (R732A) appeared to strongly reduce the current amplitude, such that chloride currents could not be accurately separated from leak. When that mutant was exposed to extracellular SCN^-, a small apparent increase in current was observed. It is possible that this mutant is modifying channel conductance or channel expression; however, the inability to record chloride currents rendered electrophysiological characterizations difficult, and therefore, we did not study it further. To assess the possibility that the observed shifts in permeability ratios might result from downstream effects of an allosteric effect on gating, we tested the calcium sensitivity of the five mutants in inside-out patches and found that, although four mutants (R511A, K599A, R617A, and R784A) produced no significant effects on apparent calcium sensitivity, K641A produced a strong leftward shift in EC_{50} for calcium-dependent activation (94 nM compared with 966 nM for the WT) (Fig. S1); therefore, we excluded it from additional analysis.

In one of the original studies to identify TMEM16A as a CaCC, the selectivity of the *Xenopus* TMEM16A was dynamically modulated by the concentration of intracellular calcium, suggesting the possibility that multiple open states might exist with differentiable permeation properties (3). More recently, studies of TMEM16B have shown that anion permeation seems to be linked with calcium dependence (25, 26). To test the contribution of intracellular calcium to the selectivity properties of TMEM16A, we performed ramp protocols similar to those used at 1.7 μM $[Ca^{2+}]_i$ (Fig. 1*B*) but at lower (400 nM) (Fig. 2*A*) and higher (1 mM) intracellular calcium (Fig. 2*B*). TMEM16A shows an outward rectifying or voltage-dependent current at 400 nM $[Ca^{2+}]_i$ and an Ohmic, nonvoltage-dependent current at 1 mM $[Ca^{2+}]_i$, consistent with known behavior. Permeability ratios were then calculated from these recordings and plotted against those recorded for 1.7 μM $[Ca^{2+}]_i$. We found that selectivity for larger anions was significantly higher at the lowest concentration of calcium, whereas ratios at 1.7 μM and 1 mM $[Ca^{2+}]_i$ were indistinguishable (Fig. 2*C*). At 400 nM $[Ca^{2+}]_i$, the permeability ratios of mutant channels were comparable with those of the WT (Fig. 2*D*, P_{SCN}/P_{Cl}). In contrast, at 1 mM $[Ca^{2+}]_i$, alanine substitution for R511, K599, R617, or R784 significantly increased the preference for thiocyanate ions over chloride (Fig. 2*E*), suggesting that these mutants preferentially altered the permeation properties attributable to the open state conferred by high intracellular calcium concentrations.

The recent crystal structure of a TMEM16 family member from *N. hematococcus* fungus (27), albeit one ostensibly incapable of conducting anions, presents an opportunity to put these functional results into context on a hypothetical structural framework. The four color-coded basic residues important for TMEM16A anion selectivity are placed on the background of the nhTMEM16

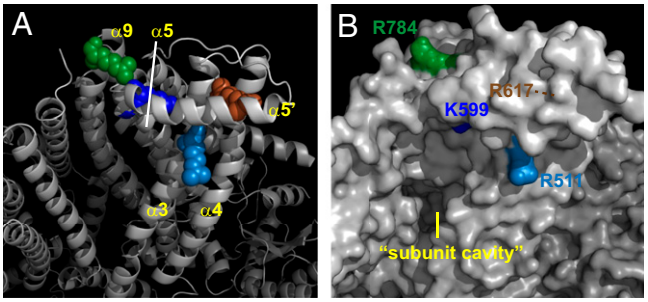

Fig. 3. Basic residues crucial for TMEM16A anion selectivity correspond to residues of nhTMEM16 that cluster around the external mouth of the subunit cavity. (*A*) Cartoon mode image of nhTMEM16 with secondary structures indicated (27) and residues corresponding to the four TMEM16A basic residues as per sequence alignment replaced with the basic residues as in mTMEM16A and colored as per Fig. 1*A* (RCSB Protein Data Bank ID code 4WIS; image generated in PyMol). (*B*) Surface map of the same view as in *A*.

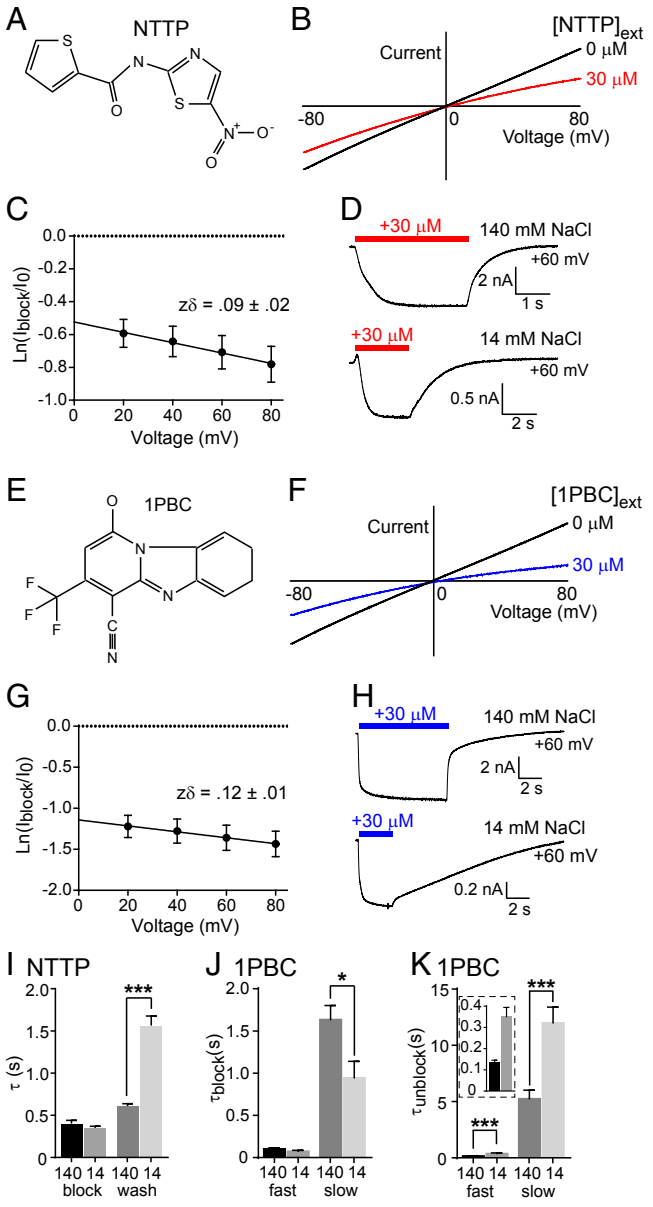

Fig. 4. Characterization of two pore blockers from a high-throughput small molecule screen. (*A*) Structure of TMEM16A inhibitor (PubChem SID 50085892) NTTP. (*B*) Representative currents recorded from voltage ramps from −80 to +80 mV in whole-cell patch clamp for TMEM16A in NaCl bath solution (black trace) and bath solution with 30 μM NTTP (red trace). (*C*) Voltage dependence of block is calculated at positive potentials from the Woodhull equation, and effective block distance from the external face is shown as *zδ*. (*D*) Sample traces showing blocker onset and washout in (*Upper*) 140 mM NaCl solution and (*Lower*) low ionic solution containing 14 mM NaCl supplemented with sucrose. (*E*) Structure of TMEM16A inhibitor (PubChem SID 49642647) 1PBC. (*F*) Representative currents recorded from voltage ramps from −80 to +80 mV in whole-cell patch clamp for TMEM16A in NaCl bath solution (black trace) and bath solution with 30 μM 1PBC (blue trace). (*G*) Voltage dependence of block is calculated at positive potentials from the Woodhull equation. (*H*) Sample traces showing blocker onset and washout when membrane potential is held at +60 mV in (*Upper*) 140 mM NaCl solution and (*Lower*) low ionic solution containing 14 mM NaCl supplemented with sucrose. (*I*) Time constants fit to traces in *D* for block and unblock on washout of NTTP. (*J*) Time constants from double exponentials fit to blocking time course for traces in *I* for 1PBC with either 140 or 14 mM NaCl. (*K*) Time constants from double exponentials fit to unblock time course for traces in *I*. *K*, *Inset* shows expanded view of comparison of fast time constants. ***$P < 0.001$, *$P < 0.05$. Ln, natural logarithm.

structure [Research Collaboratory for Structural Bioinformatics (RCSB) Protein Data Bank ID code 4WIS] based on the sequence alignment as proposed (27), on a cartoon representation of the crystal structure backbone (Fig. 3*A*), and in a space-filling model (Fig. 3*B*). It is likely that conformational differences exist between this region of the TMEM16A channel and the snapshot of the nhTMEM16 protein based on both the sequence variability and the fact that the larger basic residues seem certain to render the hypothetical structure to be energetically unfavorable as shown. However, it is striking that these basic residues correspond to residues that cluster near the outer mouth of a hydrophilic invagination in the crystal structure (27). Consistent with previous assertions of predicted channel topology (17, 19, 29), we propose that this arc of basic residues is located at the outer mouth of a pore and that increases in intracellular calcium likely cause conformational changes in this region so as to modify the permeation properties of the anion pore.

To probe the properties of this channel further, we examined the results from a high-throughput small molecule screen (PubChem Assay ID code 588511) for compounds that inhibit TMEM16A in such a way to indicate that they may interact with the anion pore (*SI Methods* and Fig. S2). This study used a similar methodology to previous screens, which took advantage of YFP fluorescence quenching by halide ions to identify compounds that perturb iodide influx through activated TMEM16A channels (2, 34, 36). We selected 250 compounds for secondary validation, of which we highlight the properties of two especially potent channel blockers. These compounds [PubChem substance ID (SID) 50085892, *N*-(5-nitro-1,3-thiazol-2-yl)-2-thiophenecarboxamide (NTTP) (Fig. 4*A*); PubChem SID 49642647, 1-hydroxy-3-(trifluoromethyl)pyrido[1,2-a]benzimidazole-4-carbonitrile (1PBC) (Fig. 4*E*)] blocked TMEM16A channels in the micromolar range and were both mildly but distinctly voltage-dependent (Fig. 4 *C* and *G*), suggesting that they inhibited the channel from within the voltage field. When channels were exposed to 30 μM of either blocker in 140 mM extracellular NaCl or 14 mM NaCl (supplemented with sucrose to maintain solution osmolality) at a constant membrane voltage of +60 mV, we found that the washout of both blockers was strongly diminished in the presence of the lower concentration of ions (Fig. 4 *D* and *H*), indicating that interactions of these blockers with their binding site(s) were strongly dependent on the presence of permeating ions. For the first compound (NTTP), we found that both block and unblock were well-fit by single exponential equations (Fig. 4*I*), where the time constant (τ) of washout was significantly increased by diminishing extracellular chloride. For the second compound (1PBC), double exponentials were necessary to fit the time courses of channel block and unblock on washout, and both the fast and slow unblock time constants were significantly larger when extracellular chloride level was reduced (consistent with this observation, the fast time constant of channel block was also significantly smaller when chloride concentration was reduced) (Fig. 4 *J* and *K*). These results, taken together, suggest that these two compounds are likely pore blockers.

We then tested whether the concentration dependence of these two pore blockers was altered by the mutations determined to be important for anion selectivity. When increasing concentrations of drug NTTP were applied to WT TMEM16A, the IC_{50} at +80 mV was 32.9 μM (Fig. 5 *A* and *B*). When the same compound was applied to the four mutants, the concentration dependence was significantly shifted. For R617A and R784A mutant channels, the drug blocked at much lower concentrations (4.3 and 10.0 μM, respectively). Conversely, R511A and K599A mutant channels yielded shallower and slightly right-shifted concentration dependence curves for this drug, with IC_{50} at 41.4 and 43.7 μM, respectively. When increasing concentrations of drug 1PBC were applied, the IC_{50} for WT channels was 13.1 μM (Fig. 5 *C* and *D*). Again, R617A and R784A conferred greater

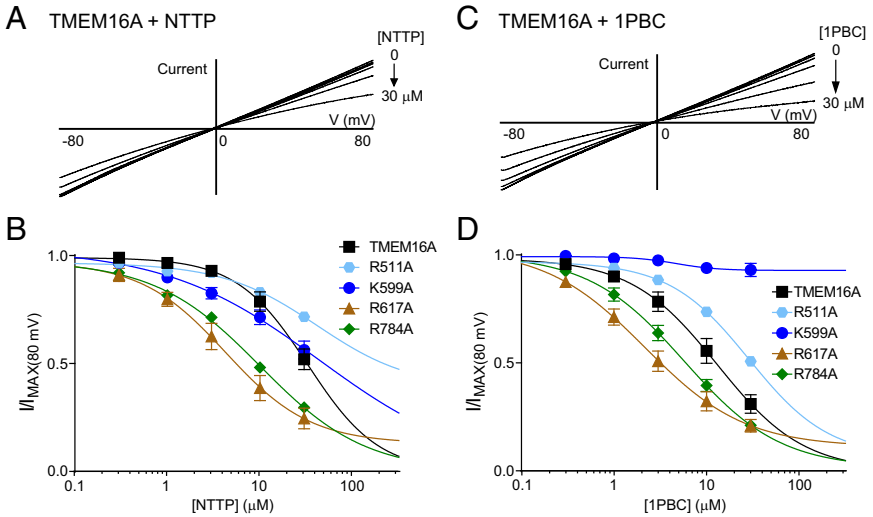

Fig. 5. Alanine mutants that alter anion selectivity also affect potency of pore blockers. (*A*) Representative currents recorded from voltage ramps from −80 to +80 mV in whole-cell patch clamp for TMEM16A in NaCl bath solution with increasing concentrations of blocker NTTP as indicated. (*B*) Concentration–response curves are plotted for NTTP for TMEM16A and alanine mutants that alter anion selectivity. (*C*) Representative currents recorded from voltage ramps from −80 to +80 mV in whole-cell patch clamp for TMEM16A in NaCl bath solution with increasing concentrations of blocker 1PBC as indicated. (*D*) Concentration–response curves are plotted for 1PBC for TMEM16A and alanine mutants that alter anion selectivity.

potency to the drug compared with the WT (IC_{50} of 2.2 and 5.8 μM). Notably, whereas R511A shifted the IC_{50} rightward for this drug as well (28.9 μM), K599A appeared to completely abolish block, because we were unable to observe any change in current amplitude up to 30 μM compared with bath solution alone. This finding could reflect either an inability of the drug to interact with the mutant channel or a loss of the drug action in blocking the-mutant channel pore, because the drug potency could be affected by a direct effect of the mutant channel conformation on the blocker binding site or an indirect effect on the blocker caused by altered pore properties. Because the TMEM16A channel pore appears to have multiple possible conductive conformations, we also examined the blocking properties of the two compounds of interest on WT channels with varying calcium concentrations (Fig. S3). These drugs seemed to block progressively more effectively at increasing calcium levels, with a mild effect exhibited by NTTP (IC_{50} = 54.0, 32.9, and 23.7 μM, respectively) and a more marked effect displayed by 1PBC (IC_{50} = 30.9, 13.1, and 8.6 μM, respectively) at 400 nM, 1.7 μM, and 1 mM intracellular calcium. This observation suggests that 1PBC may have some preference for the high calcium open state.

Discussion

To study the mechanism by which anions traverse the membrane through TMEM16A channels, we identified basic residues important for anion selectivity as well as pharmacological tools to probe that conductance pathway. By placing these four basic residues onto their corresponding positions of a recent crystal structure of a fungal TMEM16 family member (27), we found that they cluster around the outer mouth of a suggested pore region from that structure. Although the mechanism by which anions permeate the pore requires additional investigation, it is tempting to speculate that the presence of the positively charged side chains of these residues might preferentially promote flux of the smaller and more electronegative chloride ions given that the crystal structure is in its calcium-bound and presumably, fully active state (27), where chloride ions tend to flow best. These results are also consistent with previous findings that permeant ions influence the gating process (25, 26). If the open state of the pore at low Ca^{2+} is more selective to thiocyanate, as shown in Fig. 2 *D* and *E*, then the concentration of intracellular calcium necessary to reach the maximal open probability for the thiocyanate ion would seem to be less as a result, which is reported in refs 25 and 26. Interestingly, a physiological role for the preference for thiocyanate may exist for these channels, where thiocyanate may be transported across the apical membrane of airway epithelial cells through CaCCs and converted to $OSCN^-$ by a combination of oxidases, such as Duox and lactoperoxidase, as an innate immunity defense mechanism against pathogens (38). On the same note, iodide ions are also strongly selected for over chloride, which may be relevant for ensuring proper thyrocyte function in humans and rats (39).

In addition to identifying key residues for anion selectivity, we also identified pore blockers with potency that was affected by mutations at these basic residues. These two compounds were both identified from a high-throughput small molecule screen for TMEM16A inhibitors, and both seem to block in the low micromolar range. Of four residues important for anion selectivity, alanine substitution for R617 and R784 actually increased blocker potency, whereas alanine substitution for the other two basic residues seemed to weaken or abolish channel block by these compounds. Our results are consistent with the possibility that these drugs may block the permeation pore, such that mutations that reduce chloride interaction with the putative pore-lining basic residues may reduce electrostatic or steric repulsion on a drug in its binding site. R511A and K599A, however, may, in fact, be part of the binding site itself, because both of these mutants produce significant losses in blocker potency compared with WT channels. Although it is not yet possible to know exactly where the voltage field would be in this channel, the observation that the drugs blocked the pore at ∼10% of the electric field from the extracellular face is consistent with the projected locations of these residues to the external mouth of the subunit cavities of the nhTMEM16 crystal structure (27).

In conclusion, we have shown that basic residues in the putative pore region are strong determinants of anion selectivity in the TMEM16A CaCC. These residues seem to underlie a more chloride-friendly open state of the channel adopted with greater calcium concentrations than those required to minimally activate the channel, consistent with previous observations (3). We have also identified two pore blockers that seem to interact in the region of the channel containing the basic residues important for

anion selectivity, implicating this region as the likely pore. These two compounds along with the existing body of pharmacological modulators of this channel will be useful for additional structural and functional characterization of the TMEM16A channel and its family members.

Methods

Cell Culture and Molecular Biology. HEK293 cells were maintained in DMEM (Gibco) supplemented with 10% (vol/vol) FBS and 0.1% penicillin-streptomycin at 37 °C and 5% CO_2. Transfections were performed in the same media without antibiotics with Fugene6 (Promega) as per the manufacturer's instructions 24–48 h before recording. mTMEM16A was cloned into pEGFP-N1 (Clontech), and represents the splice variant-a of the gene (37). Site-directed mutagenesis was performed using the Quickchange Kit with *Pfuturbo* Polymerase (Agilent).

Electrophysiology. Twenty-four to forty-eight hours after transfection, HEK293 cells were lifted from their culture dishes with 0.05% trypsin-EDTA and plated onto poly-L-lysine–coated coverslips. After allowing the cells to settle for at least 1 h, coverslips were transferred to a recording chamber on a Nikon-TE2000 Inverted Scope, and cells were visualized with an Andor Clara Camera with Metamorph software (Molecular Devices) to confirm transfection using eGFP. Whole-cell patch-clamp recordings were performed using borosilicate capillary glass electrodes (Sutter Instrument) polished to a tip resistance of 3–5 MΩ. Inside-out patch-clamp recordings used electrodes polished to a resistance of 2–3 MΩ. Data were acquired using an Axopatch 700B Patch-Clamp Amplifier and Digidata 1440 Digitizer with pClamp10 software (Molecular Devices). All experiments were performed at room temperature (22–24 °C).

Solutions. Whole-cell electrophysiology recordings were performed using a standard bath solution containing 140 mM NaCl, 10 mM Hepes, 5 mM EGTA, pH 7.2 (NaOH). For extracellular bi-ionic experiments, NaCl was replaced with 140 mM NaBr, NaI, or NaSCN. When lower concentrations of extracellular ions were necessary, 140 mM NaCl was replaced by 14 mM NaCl and 252 mM sucrose to preserve isotonic osmolarity. Whole-cell intracellular solutions contained 140 mM NaCl, 10 mM Hepes, and 2 mM $MgCl_2$, pH 7.2 plus 5 mM EGTA, which had been previously titrated to the desired free calcium concentration with $Ca(OH)_2$. Calcium concentrations were estimated before titration using a CaBuf prediction software from Guy Droogmans, Department of Physiology, Katholieke Universiteit Leuven, Leuven, Belgium, and confirmed using Fura dyes and a calcium calibration kit (Invitrogen); 1 mM Ca^{2+} intracellular solution was generated by omitting EGTA and adding 1 mM $CaCl_2$ directly to calcium-buffer free solution. For inside-out patch clamp recordings, the extracellular bath solution was supplemented with 2 mM $MgCl_2$ for the pipette solution, whereas a series of intracellular solutions with varying concentrations of calcium was generated as described for the whole-cell internal solution. For drug block recordings, drugs (Chembridge) were added to bath solution at the highest concentration used (30 μM) and then, diluted to the desired concentration.

Data Analysis. All data were analyzed using pClamp10, Microsoft Excel, and Graphpad Prism software. Detailed descriptions of our data fitting are in *SI Extended Data Analysis*.

ACKNOWLEDGMENTS. We appreciate the assistance of Meng Wu and Zhihong Lin for the assay development and implementation of the primary high-throughput screen. C.J.P. received funding from a Heart & Stroke Foundation of British Columbia and the Yukon Research Fellowship. J.T. received funding from National Institutes of Health (NIH) Grant 5F31NS076180. Y.N.J. and L.Y.J. are Howard Hughes Medical Institute Investigators. M.L. received funding from the NIH and Molecular Libraries Probe Production Centers Network Grant U54MH084691. L.Y.J. received funding from NIH Grant R01NS069229.

1. Yang YD, et al. (2008) TMEM16A confers receptor-activated calcium-dependent chloride conductance. *Nature* 455(7217):1210–1215.
2. Caputo A, et al. (2008) TMEM16A, a membrane protein associated with calcium-dependent chloride channel activity. *Science* 322(5901):590–594.
3. Schroeder BC, Cheng T, Jan YN, Jan LY (2008) Expression cloning of TMEM16A as a calcium-activated chloride channel subunit. *Cell* 134(6):1019–1029.
4. Pifferi S, Dibattista M, Menini A (2009) TMEM16B induces chloride currents activated by calcium in mammalian cells. *Pflugers Arch* 458(6):1023–1038.
5. Huang F, et al. (2009) Studies on expression and function of the TMEM16A calcium-activated chloride channel. *Proc Natl Acad Sci USA* 106(50):21413–21418.
6. Huang F, et al. (2012) Calcium-activated chloride channel TMEM16A modulates mucin secretion and airway smooth muscle contraction. *Proc Natl Acad Sci USA* 109(40): 16354–16359.
7. Ousingsawat J, et al. (2009) Loss of TMEM16A causes a defect in epithelial Ca2+-dependent chloride transport. *J Biol Chem* 284(42):28698–28703.
8. Romanenko VG, et al. (2010) Tmem16A encodes the Ca2+-activated Cl- channel in mouse submandibular salivary gland acinar cells. *J Biol Chem* 285(17):12990–13001.
9. Zhu MH, et al. (2009) A Ca(2+)-activated Cl(-) conductance in interstitial cells of Cajal linked to slow wave currents and pacemaker activity. *J Physiol* 587(Pt 20):4905–4918.
10. Cho H, et al. (2012) The calcium-activated chloride channel anoctamin 1 acts as a heat sensor in nociceptive neurons. *Nat Neurosci* 15(7):1015–1021.
11. Jeon JH, Paik SS, Chun MH, Oh U, Kim IB (2013) Presynaptic localization and possible function of calcium-activated chloride channel anoctamin 1 in the mammalian retina. *PLoS ONE* 8(6):e67989.
12. Jeon JH, et al. (2011) Expression and immunohistochemical localization of TMEM16A/anoctamin 1, a calcium-activated chloride channel in the mouse cochlea. *Cell Tissue Res* 345(2):223–230.
13. Huang WC, et al. (2012) Calcium-activated chloride channels (CaCCs) regulate action potential and synaptic response in hippocampal neurons. *Neuron* 74(1):179–192.
14. Sancho M, García-Pascual A, Triguero D (2012) Presence of the Ca2+-activated chloride channel anoctamin 1 in the urethra and its role in excitatory neurotransmission. *Am J Physiol Renal Physiol* 302(3):F390–F400.
15. Davis AJ, et al. (2010) Expression profile and protein translation of TMEM16A in murine smooth muscle. *Am J Physiol Cell Physiol* 299(5):C948–C959.
16. Duvvuri U, et al. (2012) TMEM16A induces MAPK and contributes directly to tumorigenesis and cancer progression. *Cancer Res* 72(13):3270–3281.
17. Yu K, Duran C, Qu Z, Cui YY, Hartzell HC (2012) Explaining calcium-dependent gating of anoctamin-1 chloride channels requires a revised topology. *Circ Res* 110(7):990–999.
18. Yu K, Zhu J, Qu Z, Cui YY, Hartzell HC (2014) Activation of the Ano1 (TMEM16A) chloride channel by calcium is not mediated by calmodulin. *J Gen Physiol* 143(2): 253–267.
19. Tien J, et al. (2014) A comprehensive search for calcium binding sites critical for TMEM16A calcium-activated chloride channel activity. *eLife* 3:3.
20. Kuruma A, Hartzell HC (1999) Dynamics of calcium regulation of chloride currents in Xenopus oocytes. *Am J Physiol* 276(1 Pt 1):C161–C175.
21. Kuruma A, Hartzell HC (2000) Bimodal control of a Ca(2+)-activated Cl(-) channel by different Ca(2+) signals. *J Gen Physiol* 115(1):59–80.
22. Boton R, Dascal N, Gillo B, Lass Y (1989) Two calcium-activated chloride conductances in Xenopus laevis oocytes permeabilized with the ionophore A23187. *J Physiol* 408: 511–534.
23. Perez-Cornejo P, De Santiago JA, Arreola J (2004) Permeant anions control gating of calcium-dependent chloride channels. *J Membr Biol* 198(3):125–133.
24. Lupu-Meiri M, Shapira H, Oron Y (1989) Dual regulation by protein kinase C of the muscarinic response in Xenopus oocytes. *Pflugers Arch* 413(5):498–504.
25. Sagheddu C, et al. (2010) Calcium concentration jumps reveal dynamic ion selectivity of calcium-activated chloride currents in mouse olfactory sensory neurons and TMEM16b-transfected HEK 293T cells. *J Physiol* 588(Pt 21):4189–4204.
26. Betto G, et al. (2014) Interactions between permeation and gating in the TMEM16B/anoctamin2 calcium-activated chloride channel. *J Gen Physiol* 143(6):703–718.
27. Brunner JD, Lim NK, Schenck S, Duerst A, Dutzler R (2014) X-ray structure of a calcium-activated TMEM16 lipid scramblase. *Nature* 516(7530):207–212.
28. Yang H, et al. (2012) TMEM16F forms a Ca2+-activated cation channel required for lipid scrambling in platelets during blood coagulation. *Cell* 151(1):111–122.
29. Bill A, et al. (2015) Variomics screen identifies the re-entrant loop of the calcium-activated chloride channel ANO1 that facilitates channel activation. *J Biol Chem* 290(2):889–903.
30. Namkung W, Thiagarajah JR, Phuan PW, Verkman AS (2010) Inhibition of Ca2+-activated Cl- channels by gallotannins as a possible molecular basis for health benefits of red wine and green tea. *FASEB J* 24(11):4178–4186.
31. Liu Y, et al. (2014) Characterization of the effects of Cl– channel modulators on TMEM16A and bestrophin-1 Ca2+ activated Cl– channels. *Pflugers Arch*, 10.1007/s00424-014-1572-5.
32. Bradley E, et al. (2014) Pharmacological characterization of TMEM16A currents. *Channels (Austin)* 8(4):308–320.
33. Sanders KM, O'Driscoll K, Leblanc N (2014) Pharmacological properties of native CaCCs and TMEM16A. *Channels (Austin)*, 86, pp 473–474.
34. De La Fuente R, Namkung W, Mills A, Verkman AS (2008) Small-molecule screen identifies inhibitors of a human intestinal calcium-activated chloride channel. *Mol Pharmacol* 73(3):758–768.
35. Reyes JP, et al. (2014) Anion permeation in calcium-activated chloride channels formed by TMEM16A from Xenopus tropicalis. *Pflugers Arch* 466(9):1769–1777.
36. Namkung W, Phuan PW, Verkman AS (2011) TMEM16A inhibitors reveal TMEM16A as a minor component of calcium-activated chloride channel conductance in airway and intestinal epithelial cells. *J Biol Chem* 286(3):2365–2374.
37. Ferrera L, et al. (2009) Regulation of TMEM16A chloride channel properties by alternative splicing. *J Biol Chem* 284(48):33360–33368.
38. Rada B, Leto TL (2008) Oxidative innate immune defenses by Nox/Duox family NADPH oxidases. *Contrib Microbiol* 15:164–187.
39. Twyffels L, et al. (2014) Anoctamin-1/TMEM16A is the major apical iodide channel of the thyrocyte. *Am J Physiol Cell Physiol* 307(12):C1102–C1112.